PCCP

Confinement boosts CO oxidation on Ni atom embedded inside boron nitride nanotubes

Journal:	*Physical Chemistry Chemical Physics*
Manuscript ID	CP-ART-03-2018-001957
Article Type:	Paper
Date Submitted by the Author:	27-Mar-2018

Complete List of Authors:	Zhang, Yadong; Nanjing University of Science and Technology, Liu, Yuzhen; Nanjing University of Science and Technology, Meng, Zhaoshun; Nanjing University of Science and Technology, Ning, Cai; Nanjing University of Science and Technology, Applied Physics Xiao, Chuanyun; Nanjing University of Science and Technology, Deng, Kaiming; Nanjing University of Science and Technology, Jena, Purusottam; Virginia Commonwealth University, Physics Department Lu, Ruifeng; Nanjing University of Science and Technology, Applied Physics

Journal Name

ARTICLE

Confinement boosts CO oxidation on Ni atom embedded inside boron nitride nanotubes†

Received 00th January 20xx,
Accepted 00th January 20xx

DOI: 10.1039/x0xx00000x

www.rsc.org/

Yadong Zhang,[‡a] Yuzhen Liu,[‡a] Zhaoshun Meng,[a] Cai Ning,[a] Chuanyun Xiao,[a] Kaiming Deng,[a] Purusottam Jena*[b] and Ruifeng Lu*[a,c]

To date, most studies of heterogeneous catalysis have focused on metal particles supported on the surface of substrates. However, studies of catalytic properties of metallic nanoparticles supported on the interior surface of nanotubes are rare. Using first-principles calculations based on density functional theory, we have studied the CO oxidation on a single nickel atom confined in a nitrogen vacancy on the inside surface of boron nitride nanotubes (BNNT). By exploring the Eley-Rideal mechanism, we find that Ni atom embedded on the interior surface of BNNTs exhibits a much higher catalytic activity for CO oxidation when compared with Ni doped on its outside surface. In addition, the energy barriers of the rate-determining step for CO oxidation on Ni embedded on the inside wall of BNNT(5, 5), BNNT(6, 6) and BNNT(7, 7) are 0.39, 0.29 and 0.33 eV, respectively. The results illustrate the merit of confinement on CO oxidation.

Introduction

Carbon monoxide, a colorless, odorless, and tasteless gas, is mainly emitted from automobiles, power plants, industrial, and domestic activities.[1-4] Due to its high affinity with hemoglobin, carbon monoxide is a lethal gas for humans and animals when encountered in concentrations above 650 ppm.[5] Besides, it is also flammable, when the concentration exceeds 12 vol%.[1] Even a small amount of carbon monoxide (>10 ppm), present in the hydrogen-rich gas mixture, poisons the fuel cell electrodes.[6] This is particularly important in hydrogen fuel cells, which are an alternative to conventional fossil fuels. Note that carbon monoxide is an unavoidable byproduct[7,8] when hydrogen gas is produced from steam reforming or partial oxidation of hydrocarbons. Therefore, for fuel cell applications, selective catalytic oxidation of CO to CO_2 is the most effective and economical way to remove trace amount of CO from hydrogen or air.

In the past, a number of catalysts have been proposed for the preferential oxidation of CO in hydrogen-rich gas mixture. Some noble metal containing catalysts, such as Pt,[4,9,10] Pt-Co alloy,[11] Pd,[12-14] Rh,[15,16] and Au[17-20] can catalyze CO oxidation effectively. However, considerable cost, requirement of high reaction temperatures and low abundance hinder their larger-scale applications. Nanoscience and nanotechnology provide opportunities and strategies for the design of novel catalysts.[21-24] Both experimental and theoretical works have demonstrated the importance of particle size in the performance of catalysts.[25,26] With decreasing size of supported metal particles, surface to volume ratio increases and the coordination number decreases. These effects, combined with quantum confinement, enable nanoparticles to become increasingly active in specific reactions. Thus, downsizing the particle size to few-atom clusters and ultimately to a single atom is highly desirable for developing nanocatalysists.[27-30]

Recently, there is considerable interest, both experimentally and theoretically, to develop single-atom catalysts. For example, Zhang and co-workers[28] fabricated a novel catalyst with a single Pt atom anchored on iron oxide (FeO_x) nano crystallites, exhibiting very high activity and stability for CO oxidation. Diebold and co-workers[30] reported the stabilization of single Ni atom on a two-dimensional (2D) titania structure with periodic six- and ten-membered nanopores, which is stable even at room temperature. In addition, research has shown that some metal oxides (such as Al_2O_3,[31,32] CeO_2,[33,34] TiO_2,[35] Co_3O_4,[36] ZnO,[37] and MnO_2[38]) and metals (such as Cu[39] and Ag[40]) are promising substrates for single atom catalysis. Besides traditional metal oxides and metals, single atom catalysts supported on 2D substrates, such as graphene,[41-46] graphene oxide,[47] graphyne,[48] graphitic carbon nitride (g-C_3N_4),[49] MXenes,[50] organometallic sheets,[51] C_2N monolayers,[52] polymeric phthalocyanine[3] and BN monolayers[53-58] have attracted attention due to their intrinsic high surface area and activity, efficiency, and stability. By using a modified arc-discharge method, Zhang and co-workers[59] experimentally synthesized single atom catalyst by stabilizing Nb atom in defective graphitic layers at high density. This catalyst exhibited excellent performance for the oxygen reduction

[a] Department of Applied Physics, Nanjing University of Science and Technology, Nanjing 210094, People's Republic of China. Email: rflu@njust.edu.cn
[b] Department of Physics, Virginia Commonwealth University, Richmond, Virginia 23204, United States. E-mail: pjena@vcu.edu
[c] State Key Lab of Molecular Reaction Dynamics, Dalian Institute of Chemical Physics, Chinese Academy of Sciences, Dalian 116023, People's Republic of China
†Electronic Supplementary Information (ESI) available: See DOI: 10.1039/x0xx00000x
‡These authors contributed equally to this work.

reaction. Yang and co-workers[52] systematically screened the potential of 3*d* transition metal atoms embedded in C_2N monolayers as single atom catalysts for CO oxidation. The results revealed that Cr and Mn embedded in C_2N monolayers are promising single atom catalysts for the low-temperature CO oxidation reaction.

In addition to the above studies, carbon nanotubes have been widely studied as an alternative substrate for dispersing transition metals on their exterior or interior surface for hydrogen evolution reaction, oxygen reduction reaction, and ammonia synthesis and decomposition.[60,61] Due to the difficulty in dispersing metal nanoparticles uniformly inside carbon nanotube channels, catalysts, utilizing the interior surface of nanotubes, have been less explored compared to that using exterior wall. However, recently techniques have been successfully developed to introduce metal nanoparticles into the channels of carbon nanotube, such as *in situ* filling during arc discharge, vapor deposition of volatile complexes, and wet chemistry methods.[62-65] Moreover, studies have demonstrated that confining metal nanoparticles inside carbon nanotubes often leads to a different catalytic activity, with respect to the same metal deposited on the exterior surface of carbon nanotubes.[60] For example, Bao and co-workers[66] reported a striking enhancement of the catalytic activity of Rh particles confined inside nanotubes for the conversion of CO and H_2 to ethanol. The overall formation rate of ethanol inside the nanotubes exceeds that on the outside of the nanotubes by more than one order of magnitude. Subsequently, the authors[67] studied the confinement effect on Fischer-Tropsch synthesis by comparing iron confined in multi-wall carbon nanotube and on the outside surface, and found that the Fe-confined catalyst favors CO conversion and formation of long chain hydrocarbons.

Boron nitride nanotubes (BNNTs) have well-defined hollow interior and possess many properties superior to that of carbon nanotubes such as unusual mechanical and thermal conductivity.[68,69] In addition, one can create both B and N vacancies in boron nitride nanotubes, providing additional freedom to embed metal atoms. Note that both boron and nitrogen vacancies have been experimentally identified on BN nanosheet by Jin et al.[70] via direct imaging after controlled energetic electron beam irradiation. Furthermore, Zobelli et al.[71] claimed that BNNTs are more susceptible to support a vacancy than h-BN.

In this work, we performed systematic first-principles calculations to examine the catalytic performance for CO oxidation using a single Ni atom doped substrates, including h-BN, BNNT(5, 5), BNNT(6, 6), and BNNT(7, 7). We considered Ni atom embedded on both the interior and exterior surfaces of BNNTs. We found that the O2 and CO prefer to bind to N-vacancy more strongly than to B-vacancy in h-BN and BNNT(6, 6). Thus, we mainly discuss the catalytic activity associated with the N-vacancy. Our calculations suggest that all studied Ni-$BNNTs_{N\text{-}Vacancy\text{-}in}$ exhibit high catalytic activity for CO oxidation reaction.

Computational methods

Using spin-polarized density functional theory (DFT) with generalized gradient approximation (GGA) for exchange-correlation potential, we have calculated the total energies, electronic structure, and atomic structure of Ni doped BNNT systems. All calculations were performed by using Perdew-Burke-Ernzerhof (PBE)[72,73] form of the GGA functional embedded in the Vienna Ab Initio Simulation Package (VASP).[74] The cutoff energy of the plane-wave basis set was set at 400 eV. The BNNTs with periodic boundary condition was modeled with a large super cell of 20×20×12.53 $Å^3$, eliminating the artificial interaction between nanotubes in adjacent cells. In order to avoid interaction between periodic h-BN layers, a vacuum space of 15 Å along the *z*-direction was applied. The convergence thresholds for structural optimization and transition state (TS) search were set at 0.01 eV in energy and 0.05 eV/Å in force, respectively. The convergence criterion for energy is 10^{-5} eV. The Brillouin zone integrations are performed by using Monkhorst-Pack 3×3×1 and 1×1×3 grids for h-BN and BNNTs, respectively.[75] The climbing image nudged elastic band (CI-NEB) method was used to search the TSs and four or five images inserted in between two stable states.[76] The van der Waals (vdW) dispersion was included using the D3 method of Grimme.[77] We used the electro-static potential (ESP) charges[78] to compute the atomic charges, which is based on the electrostatic potential.

The binding energy (E_b) of Ni atom doped in substrate can be obtained from $E_b = E_{Ni@substrate} - E_{Ni} - E_{substrate}$, where $E_{Ni@substrate}$ is the energy of the optimized structure of single Ni atom doped in h-BN or BNNTs, E_{Ni} and $E_{substrate}$ are the energies of the isolated Ni atom and the substrate, respectively. Similarly, the adsorption energy (E_{ad}) of gas molecules (O_2 and CO) on the catalyst particle is defined as: $E_{ad} = E_{gas@catalyst} - E_{gas} - E_{catalyst}$, where $E_{gas@catalyst}$ is the energy of the optimized structure of gas molecule adsorbed on the catalyst, E_{gas} and $E_{catalyst}$ are the energies of the isolated gas molecule and the catalyst, respectively. In all cases, the negative E_b or E_{ad} value corresponds to exothermic process, which indicates that embedment of Ni atom in substrates or adsorption of gas molecules on the surface of the catalysts is energetically favorable.

Results and discussion

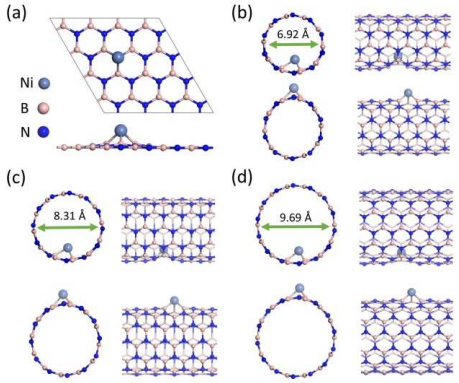

Fig. 1 The optimized structures of Ni-embedded (a) h-BN, (b) BNNT (5, 5), (c) BNNT(6, 6), and (d) BNNT (7, 7) with N vacancy.

Table 1 The optimized distance (in Å) between Ni and B or N in Ni-embedded h-BN and BNNTs, ESP charge (in *e*) and binding energy (in eV) for Ni atom at the N vacancy and B vacancy, binding energies (in eV) for O_2 and CO adsorbed at the catalyst site, and the bond length ($r_{o\text{-}o}$, in Å) of O_2 adsorbed around the Ni atom

Substrates	Ni-rim distance	E_b (Ni)	Charge (Ni)	E_b (CO)	E_b (O_2)	$r_{o\text{-}o}$
h-$BN_{B\text{-}Vacancy}$	1.79, 1.79, 1.79	−8.34	0.54	−0.71	−1.19	1.32
h-$BN_{N\text{-}Vacancy}$	1.90, 1.90, 1.90	−5.48	0.09	−1.52	−2.85	1.36
BNNT(5, 5)$_{N\text{-}Vacancy\text{-}in}$	1.85, 1.90, 1.90	−3.57	0.08	−1.39	−2.41	1.37
BNNT(5, 5)$_{N\text{-}Vacancy\text{-}out}$	1.86, 1.86, 2.00	−5.01	0.36	−1.83	−2.61	1.35
BNNT(6, 6)$_{B\text{-}Vacancy\text{-}in}$	1.78, 1.80, 1.80	−6.73	0.36	−1.20	−1.35	1.35
BNNT(6, 6)$_{B\text{-}Vacancy\text{-}out}$	1.79, 1.79, 1.84	−8.18	0.81	−1.17	−1.07	1.34
BNNT(6, 6)$_{N\text{-}Vacancy\text{-}in}$	1.85, 1.90, 1.90	−3.85	0.07	−1.54	−2.42	1.37
BNNT(6, 6)$_{N\text{-}Vacancy\text{-}out}$	1.87, 1.87, 1.98	−5.02	0.26	−1.78	−2.59	1.35
BNNT(7, 7)$_{N\text{-}Vacancy\text{-}in}$	1.86, 1.90, 1.90	−4.44	0.07	−1.69	−2.54	1.37
BNNT(7, 7)$_{N\text{-}Vacancy\text{-}out}$	1.87, 1.98, 1.98	−5.36	0.20	−1.82	−2.63	1.35

In this work, we performed systematic first-principles calculations to examine the catalytic performance for CO oxidation using a single Ni atom doped substrates, including h-BN, BNNT(5, 5), BNNT(6, 6), and BNNT(7, 7). We considered Ni atom embedded on both the interior and exterior surfaces of BNNTs. We found that the O_2 and CO prefer to bind to Ni embedded in N-vacancy more strongly than to Ni embedded in B-vacancy of h-BN and BNNT(6, 6). Thus, we mainly discuss the catalytic activity associated with the cases containing N-vacancy.

The optimized structures of a single Ni atom embedded in h-BN and BNNTs are shown in **Fig. 1**, where the Ni atom is located on top of the vacant site, forming a tetrahedral structure with three neighboring sp^3-hybridized B atom. Consistent with the pore diameter of porous nanosheet[79-81] and nanotubes[82,83] used for gas separation, we have chosen the diameters of BNNTs big enough to freely accommodate CO and O_2 molecules. The binding energies of Ni atom embedded in the B-Vacancy and N-Vacancy of h-BN and BNNTs are given in **Table 1**. The binding energies of Ni supported on the substrates with N-Vacancy can be similarly defined as those of CO and O_2. These values range from −5.48 to −3.57 eV and are smaller than the corresponding values with B-vacancy. In all cases, the binding of Ni is still strong enough to prohibit it from diffusion and aggregation at room temperature or above. In addition, the difference in ESP charge of the Ni atom trapped at the B-Vacancy and N-Vacancy, as seen in **Table 1**, is consistent with the electronegativity of B and N atoms. The more electronegative N atoms adjacent to B-vacancy attract more electrons from the Ni atom. When confined in the N-vacancy, the Ni atom loses less electrons, thus O_2 binds stronger than CO molecule, facilitating the catalytic activity for CO oxidation. This is in good agreement with Abdel's results[84]. Therefore, h-BN and BNNTs with Ni embedded in the N-Vacancy have the potential to be good catalysts.

Table 1 also lists the bond lengths between Ni atom and neighboring B (or N) atom. According to previous studies,[3,54] the adsorption energy of O_2 on substrates should be lower than that of CO to prevent catalyst poisoning by CO. We first calculated the binding energies of O_2 and CO on the Ni atom embedded in both N and B vacancies of h-BN and BNNT(6, 6). As shown in **Table 1**, the E_{ad} values of CO adsorbed on Ni-h-$BN_{B\text{-}Vacancy}$, Ni-BNNT(6, 6)$_{B\text{-}Vacancy\text{-}in}$, and Ni-BNNT(6, 6)$_{B\text{-}Vacancy\text{-}out}$ are −0.71, −1.20, and −1.17 eV, respectively. We find that the difference in adsorption energy between CO and O_2 is no more than 0.5 eV, which may facilitate CO poisoning of the catalysts. Especially for Ni-BNNT(6, 6)$_{B\text{-}Vacancy\text{-}out}$, the adsorption energy of O_2 is −1.07 eV, which is even smaller than that for CO. Fortunately, the energy difference between CO and O_2 adsorbed on Ni-h-$BN_{N\text{-}Vacancy}$ and Ni-h-$BN_{N\text{-}Vacancy}$ is about 1 eV, which could efficiently alleviate the CO poisoning of the catalysts. Therefore, the Ni atom embedded at N-Vacancy in h-BN and BNNTs would be a better catalyst for O_2 adsorption than that when it is embedded in the B-Vacancy.

As we know, the adsorption ability of gas molecule can determine the reaction pathway of the catalyst. Too strong or too weak adsorption of gas molecules will adversely affect the catalytic activity. Thus, moderate adsorption energies of reactive gases, which may reduce the reaction barrier in a catalytic reaction, are important for CO oxidation. The adsorption of the O_2 and CO molecules on the Ni atom embedded in N-Vacancy of h-BN and BNNTs is a prerequisite for CO oxidation reaction. To search for the most energetically favorable configuration, various initial geometries were optimized, such as the end-on and side-on sites. For O_2 adsorption, the most favorable configuration is characterized by O_2 molecule parallel to the catalyst surface, as shown in **Fig. S1** in the ESI†. The adsorption is quite strong, and the adsorption energy is in the range of −2.85 to −2.41 eV for Ni-h-$BN_{N\text{-}Vacancy}$ and Ni-BNNTs $_{N\text{-}Vacancy}$. The interaction between O_2 and catalysts would stretch the O_2 bond to 1.35-1.37 Å, as summarized in **Table 1**. These bond lengths are significantly longer than that of free oxygen molecule (1.23 Å). Interestingly, the bond length of O_2 molecule adsorbed in the interior wall of BNNTs is 1.37 Å, which is larger than that of the O_2 molecule adsorbed on the exterior surface of BNNTs. This implies high activation of Ni atom embedded on the interior wall. For the CO molecule adsorbed on Ni-h-$BN_{N\text{-}Vacancy}$ and Ni-$BNNTs_{N\text{-}Vacancy}$, the end-on configuration with C linked to Ni is

energetically the most favorable structure. As shown in **Table 1**, the adsorption energy of CO molecule adsorbed on Ni-h-$BN_{N\text{-}Vacancy}$ and Ni-$BNNTs_{N-Vacancy}$ is in the range from −1.83 to −1.39 eV, which is much weaker than the O_2 binding. Besides, the C-O bond lengths after adsorption are increased by 0.03, 0.04, 0.04, and 0.03 Å, respectively, for Ni-h-$BN_{N\text{-}Vacancy}$, Ni-BNNT(5, 5)$_{N\text{-}Vacancy\text{-}in}$, Ni-BNNT(6, 6)$_{N\text{-}Vacancy\text{-}in}$, and Ni-BNNT(7, 7)$_{N\text{-}Vacancy\text{-}in}$, in comparison with the free CO molecule (**Fig. S2**, ESI†).

For better understanding of the interaction between CO or O_2 and the catalyst, the electronic structures of these two species adsorbed on Ni-BNNT(6, 6)$_{N\text{-}Vacancy\text{-}in}$, Ni-BNNT(6, 6)$_{N\text{-}Vacancy\text{-}out}$ and Ni-h-$BN_{N\text{-}Vacancy}$ are analyzed. As shown by the density of states (DOS) (**Fig. S3a**, **Fig. S3c**, **Fig. S3e**, ESI†), the hybridization between the 3*d* orbital of Ni and 2*p* orbital of CO is weak near the Fermi level (E_F). The lack of strong hybridization between these orbitals is consistent with the relatively weak adsorption of CO at the metal site and the small change in the C-O bond length. Besides, as seen from **Table 1**, the elongation of the O-O bond in the adsorbed O_2 molecule implies strong interaction with the metal center. The DOS for the Ni-3*d* and O-2*p* orbitals of Ni-BNNT(6, 6)$_{N\text{-}Vacancy\text{-}in}$, Ni-BNNT(6, 6)$_{N\text{-}Vacancy\text{-}out}$ and Ni-h-$BN_{N\text{-}Vacancy}$ are also displayed (**Fig. S3b**, **Fig. S3d**, **Fig. S3f**, ESI†). Compared with the CO adsorption, a much more significant hybridization between the Ni-3*d* orbital and O_2-2*p* orbital near E_F can be seen, which signifies stronger adsorption of O_2. Based on the adsorption energy of reacting gas, the CO oxidation could proceed with CO pulling one oxygen atom from the adsorbed O_2 via the ER mechanism.

Due to the discrepancy in adsorption energy and the low concertation of CO in polluted air and hydrogen-rich gas mixture, it can be imagined that the Ni atom at the N-vacancy sites will be primarily covered by the adsorbed O_2 molecules, if CO and O_2 mixture is injected as the reacting gas. CO will then react with O_2. Thus, the CO oxidation on these catalysts should happen via a two-step ER reaction. The ER reaction proceeds as follows: (1) $CO(freestate)+O_2(adsorbedstate)\xrightarrow{catalyst}CO_2+O(adsorbedstate)$ and (2) $CO\,(free\ state\,)+O(adsorbed\ \ state\,)\xrightarrow{catalyst}CO_2$. Thus formed CO_2 molecules will automatically desorb in an exothermic process. The configurations for the initial state (IS), transition state (TS), and finial state (FS) along the reaction path for the whole CO oxidation reaction on the Ni-BNNT (6, 6)$_{N\text{-}Vacancy\text{-}in}$ are displayed in **Fig. 2**. At the IS1, a CO molecule is physisorbed far away from the pre-adsorbed O_2. For IS1, the O-O bond length is elongated from 1.23 Å of the isolated O_2 molecule to 1.37 Å, while CO is located in the middle of nanotube and almost remains in a line along with the adsorbed O_2. The distance between the C atom and the nearest O atom of O_2 is calculated to be 3.55 Å, indicating that CO is physisorbed at the IS1. Subsequently, the CO molecule approaches the activated O_2 to form TS1 site with the C-O distance of 1.15 Å.

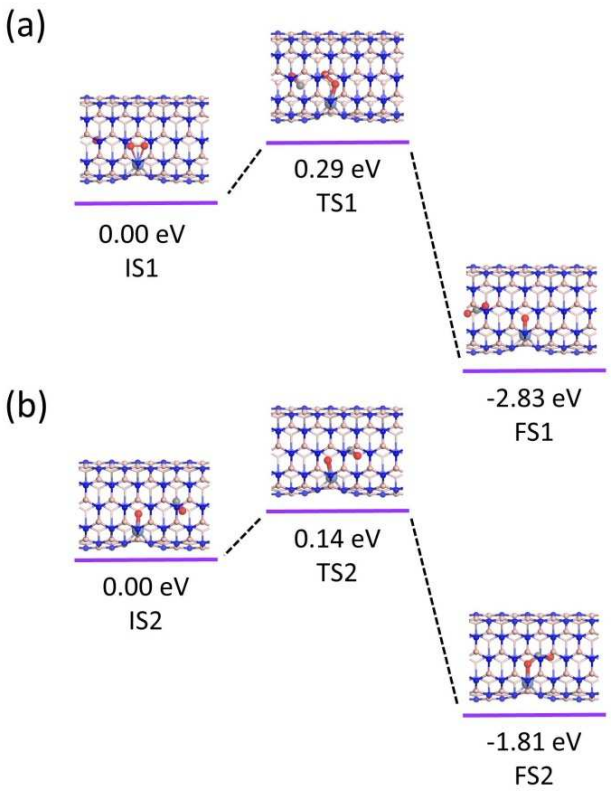

Fig. 2 Geometries (side view) and energy profiles of initial state (IS), transition state (TS), and finial state (FS) along the minimum energy path for the CO oxidation on Ni embedded in the interior wall of BNNT (6, 6) with N-Vacancy via the ER mechanisms.

At the same time, due to the confinement effect, the bond length of O_2 is reduced to 1.34 Å, which is contrary to the calculated results in other materials[52,57]. The distance between C_{CO} and O_{O2} is reduced to 2.56 Å. After reaction, a CO_2 molecule is generated with one atomic oxygen remaining above the metal atom. The large distance (4.19 Å) between the produced CO_2 molecule and the remaining O atom suggests a weak interaction between them. Thus, the molecule can desorb easily from the catalyst. This process is achieved by passing through TS1. A very low energy barrier (0.29 eV, defined as the total energy difference between the TS and the IS sites) can be overcome, breaking the O-O bond of O_2 and forming new C-O bonds. Thermodynamically, the reaction energy (defined as the total energy difference between the FS and the IS sites) of this process is exothermic by −2.83 eV, indicating that this process is energetically and kinetically favored. In the next step, the second CO molecule approaches the remaining O atom to form

the second CO_2 molecule. As shown in **Fig. 2b**, the configuration of IS2 has a weakly adsorbed CO (3.86 Å away from the remaining O atom). At the TS2, the C atom of CO combines with the O atom and the C_{CO}-O_{O2} distance is 2.44 Å. At the FS2, a CO_2 molecule is produced above the metal center. The energy barriers of the second ER step is about 0.14 eV and the reaction energy of this step is −1.81 eV, indicating this process is also exothermic. Since the energy released in this process is comparable to the adsorption energy (−0.43 eV) of CO_2 on catalyst, desorption of the CO_2 molecule from FS2 is possible in experiments.

To address the electronic interaction associated with the catalytic activity of the Ni-BNNT(6, 6)$_{N\text{-}Vacancy\text{-}in}$, we calculated the local DOS projected onto the C-O and O-O bonds as well as the *d*-projected DOS of Ni in IS1 and TS1 sites of the ER step. As shown in **Fig. 3a**, the O_2 adsorption on Ni atom mainly originates from the interaction between Ni 3*d* orbital and O_2 2π* orbital, with notable charge transfer to O_2 2π* orbital, which can be identified from O_2's DOS contribution at the Fermi level. In contrast, the 2π* level of CO is still empty, because of the larger distance between CO and Ni. As CO gets closer to Ni, the 2π* level of CO is further populated and broadened to hybridize with Ni 3*d* state. Meanwhile, mediated by the Ni 3*d* state, the O-O 5σ level interacts strongly with the C-O 1π level, which is ancillary in weakening the O-O bond and leading to the formation of C-O_{O2} bond.

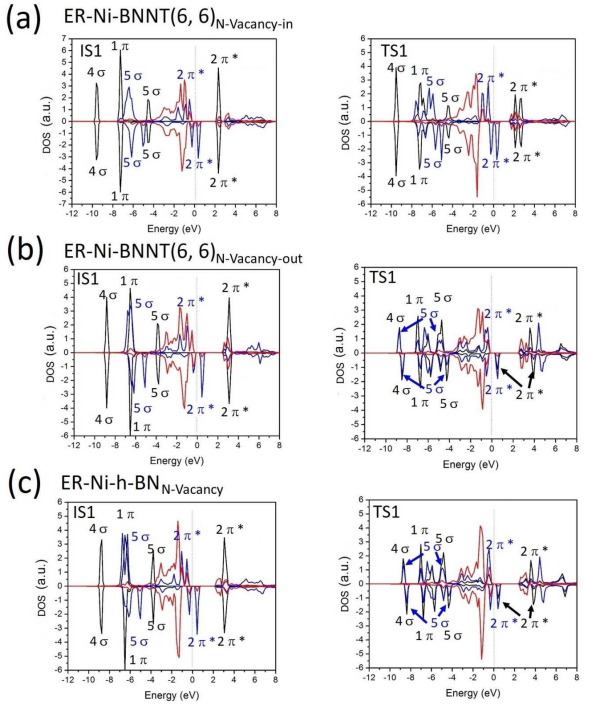

Fig. 3. Spin-polarized local DOS (LDOS) projected onto C-O and O-O on Ni-BNNT(6, 6)$_{N\text{-}vacancy\text{-}in}$, Ni-BNNT(6, 6)$_{N\text{-}vacancy\text{-}out}$, and Ni-h-BN $_{N\text{-}vacancy}$, as well as the *d*-projected DOS of Ni in the IS and TS configurations of the ER step. Black solid curves are the LDOSs projected onto C-O; blue solid curves are the LDOSs projected onto O-O; red solid curves are the *d*-projected DOSs of the Ni atom.

Table 2 The calculated energies (in eV) of TS, and FS structures relative to the energies of initial states (all E_{IS1} and E_{IS2} are set to 0) for the two reaction steps with ER mechanism. Thus, E_{TS1} and E_{TS2} correspond to energy barriers

Catalysts	E_{TS1}	E_{FS1}	E_{TS2}	E_{FS2}
Ni-h-BN$_{N\text{-}Vacancy}$	0.68	−2.62	0.10	−1.76
Ni-BNNT(5, 5)$_{N\text{-}Vacancy\text{-}in}$	0.39	−2.79	0.20	−1.57
Ni-BNNT(5, 5)$_{N\text{-}Vacancy\text{-}out}$	0.75	−2.42	0.19	−1.87
Ni-BNNT(6, 6)$_{N\text{-}Vacancy\text{-}in}$	0.29	−2.83	0.14	−1.81
Ni-BNNT(6, 6)$_{N\text{-}Vacancy\text{-}out}$	0.69	−2.44	0.11	−1.78
Ni-BNNT(7, 7)$_{N\text{-}Vacancy\text{-}in}$	0.33	−2.70	0.12	−1.70
Ni-BNNT(7, 7)$_{N\text{-}Vacancy\text{-}out}$	0.68	−2.37	0.11	−1.76

The configurations for the IS, TS, and FS sites, following the ER mechanism for the whole CO oxidation reaction on the Ni-BNNT(6, 6)$_{N\text{-}Vacancy\text{-}out}$, are displayed in **Fig. S4** in the ESI†. By comparing this catalytic process with **Fig. 2**, we find that the changes of the geometrical structures during the reaction are very different for both steps. At the IS1, due to the loss of confinement effect, the CO molecule is physically adsorbed obliquely above the pre-adsorbed O_2. The distance between the C atom and the nearer O atom of O_2 is 3.19 Å. At the TS1, the bond length of O_2 is further increased from 1.35 to 1.44 Å and the C_{CO}-O_{O2} distance is reduced to 1.65 Å, which is consistent with previous results[52,57]. As shown in Fig. S5, the energy barriers of the first and second ER steps for the CO oxidation on the Ni-BNNT(6, 6)$_{N\text{-}Vacancy\text{-}out}$ is 0.69 and 0.11 eV, respectively. In addition, the energy barriers and the reaction energies of CO oxidation catalyzed by Ni-h-BN$_{N\text{-}vacancy}$, Ni-BNNT(5, 5)$_{N\text{-}Vacancy\text{-}in}$, Ni-BNNT(5, 5)$_{N\text{-}Vacancy\text{-}out}$, Ni-BNNT(6, 6)$_{N\text{-}Vacancy\text{-}in}$, Ni-BNNT(6, 6)$_{N\text{-}Vacancy\text{-}out}$, Ni-BNNT(7, 7)$_{N\text{-}Vacancy\text{-}in}$, Ni-BNNT(7, 7)$_{N\text{-}Vacancy\text{-}out}$ are presented in **Table 2**. The energy barriers of the rate-determining step for CO oxidation on single nickel atom embedded in the interior wall of BNNT(5, 5), BNNT(6, 6) and BNNT(7, 7) are 0.39, 0.29 and 0.33 eV, respectively, which are much smaller than that of Ni-embedded on the exterior surface of BNNTs and h-BN. From these barrier values, we conclude that Ni-embedded in the N-vacancy of the interior wall of BNNTs can perform better than other catalysts such as Pt-FeO_x,[28] Cr-embedded C_2N,[52] Fe-embedded graphene,[41] Zn-embedded Pc,[3] Co–BN nanosheet,[55] Ni-embedded graphene,[46] Ru-embedded h-BN[58] and comparable with Si–BN nanosheet,[57] Ti-Ti_2CO_2,[50] Au-embedded graphene.[85]

Conclusions

In conclusion, the adsorption and catalytic behavior of Ni-embedded at the N-vacancy of h-BN nano sheet and BNNTs are investigated in detail using first-principles calculations. We found that Ni-BNNTs$_{N\text{-}Vacancy\text{-}in}$ are promising low-temperature catalysts for CO oxidation, according to the ER mechanism. Among these systems, Ni-BNNT(6, 6)$_{N\text{-}Vacancy\text{-}in}$, with the smallest reaction barrier of 0.29 eV, is the most appropriate candidate. According to previous studies,[27, 86] reactions with barriers less than 0.8 eV can proceed readily at ambient temperature. Our calculations suggest that all studied Ni-

$BNNTs_{N\text{-}Vacancy\text{-}in}$ exhibit high catalytic activity for CO oxidation reaction. This encompasses several areas of catalysis that are hotly pursued, namely, nano-confined catalysis, Ni catalysis, and single atom catalysis. We identify not only the preferred sites for CO oxidation but also the underlying mechanism associated with O-O bond stretching. We are looking forward to future experiments to confirm our theoretical prediction of the effect of confinement on catalytic behavior. We also hope that this work will stimulate further studies of other non-noble metal catalysts embedded inside BNNTs.

Acknowledgments

This work was supported by NSF of China Grant (21373113, 11374160, 21403111, 11574151), Fundamental Research Funds for the Central Universities (30916011105), Natural Science Foundation of Jiangsu Province (BK20140526, BK20170032). P. J. acknowledges support by the U.S. DOE, Office of Basic Energy Sciences, Division of Materials Sciences and Engineering under Award No. DE-FG02-96ER45579.

Notes and references

1 S. Royer and D. Duprez, *ChemCatChem*, 2011, **3**, 24-65.
2 M. L. Kimble, C. A. Jr, R. Mitrić, C. Bürgel and V. Bonacićkoutecký, *J. Am. Chem. Soc.*, 2004, **126**, 2526-2535.
3 Q. Deng, L. Zhao, X. Gao, M. Zhang, Y. Luo and Y. Zhao, *Small*, 2013, **9**, 3506-3513.
4 M. D. Ackermann, T. M. Pedersen, B. L. Hendriksen, O. Robach, S. C. Bobaru, I. Popa, C. Quiros, H. Kim, B. Hammer and S. Ferrer, *Phys. Rev. Lett.*, 2005, **95**, 255505-255508.
5 R. A. Jones, J. A. Strickland, J. A. Stunkard and J. Siegel, *Toxicol. Appl. Pharmacol.*, 1971, **19**, 46-53.
6 G. A. Camara, E. A. Ticianelli, S. Mukerjee, S. J. Lee and J. McBreen, *J. Electrochem. Soc.*, 2002, **149**, A748-A753.
7 S. Huang, K. Hara and A. Fukuoka, *Energ. Environ. Sci.*, 2009, **2**, 1060-1068.
8 R. J. Farrauto, Y. Liu, W. Ruettinger, O. Ilinich, L. Shore and T. Giroux, *Catal. Rev.*, 2007, **49**, 141-196.
9 A. Alavi, P. Hu, T. Deutsch, P. L. Silvestrellij Uuml and R. Hutter, *Phys. Rev. Lett.*, 1998, **80**, 3650-3653.
10 S. W. Lee, S. Chen, W. Sheng, N. Yabuuchi, Y. T. Kim, T. Mitani, E. Vescovo and Y. Shao-Horn, *J. Am. Chem. Soc.*, 2009, **131**, 15669-15677.
11 Y. Gauthier, M. Schmid, S. Padovani, E. Lundgren, V. Bus, G. Kresse, J. Redinger and P. Varga, *Phys. Rev. Lett.*, 2001, **87**, 36103-36107.
12 S. H. Oh and G. B. Hoflund, *J. Catal.*, 2007, **245**, 35-44.
13 C. J. Zhang and and P. Hu, *J. Am. Chem. Soc.*, 2001, **123**, 1166-1172.
14 P. Salo, K. Honkala, M. Alatalo and K. Laasonen, *Surf. Sci.*, 2002, **516**, 247-253.
15 D. J. Liu, *J. Phys. Chem. C*, 2007, **111**, 14698-14706.
16 A. Eichler, *Surf. Sci.*, 2002, **498**, 314-320.
17 Z. P. Liu, X. Q. Gong, J. Kohanoff, C. Sanchez and P. Hu, *Phys. Rev. Lett.*, 2004, **91**, 266102-266105.
18 N. Lopez and J. K. Nørskov, *J. Am. Chem. Soc.*, 2002, **124**, 11262-11263.
19 W. T. Wallace and R. L. Whetten, *J. Am. Chem. Soc.* , 2002, **124**, 7499-7505.
20 I. N. Remediakis, N. Lopez and J. K. Nørskov, *Angew. Chem. Int. Ed.*, 2005, **44**, 1824-1826.
21 M. Turner, V. B. Golovko, O. P. Vaughan, P. Abdulkin, A. Berenguer-Murcia, M. S. Tikhov, B. F. Johnson and R. M. Lambert, *Nature*, 2008, **454**, 981-983.
22 M. C. Daniel and D. Astruc, *Chem. Rev.*, 2004, **104**, 293-346.
23 A. A. Herzing, C. J. Kiely, A. F. Carley, P. Landon and G. J. Hutchings, *Science*, 2008, **321**, 1331-1335.
24 M. Haruta, *Catal. Today*, 1997, **36**, 153-166.
25 K. Judai, S. Abbet, A. S. Wörz, U. Heiz and C. R. Henry, *J. Am. Chem. Soc.*, 2004, **126**, 2732-2737.
26 Y. Lei, F. Mehmood, S. Lee, J. Greeley, B. Lee, S. Seifert, R. E. Winans, J. W. Elam, R. J. Meyer and P. C. Redfern, *Science*, 2010, **328**, 224-228.
27 X. F. Yang, A. Wang, B. Qiao, J. Li, J. Liu and T. Zhang, *Acc. Chem. Res.*, 2013, **46**, 1740-1748.
28 B. Qiao, A. Wang, X. Yang, L. F. Allard, Z. Jiang, Y. Cui, J. Liu, J. Li and T. Zhang, *Nat. Chem.*, 2011, **3**, 634-641.
29 O. Miramontes, F. Bonafé, U. Santiago, E. Larios-Rodriguez, J. J. Velázquez-Salazar, M. M. Mariscal and M. J. Yacaman, *Phys. Chem. Chem. Phys.*, 2015, **17**, 7898-7906.
30 Z. Wang, X. Hao, S. Gerhold, P. Mares, M. Wagner, R. Bliem, K. Schulte, M. Schmid, C. Franchini and U. Diebold, *J. Phys. Chem. C*, 2014, **118**, 19904-19909.
31 S. Wang, A. Y. Borisevich, S. N. Rashkeev, M. V. Glazoff, K. Sohlberg, S. J. Pennycook and S. T. Pantelides, *Nat. Mater.*, 2004, **3**, 143-146.
32 J. H. Kwak, J. Hu, D. Mei, C. W. Yi, D. H. Kim, C. H. Peden, L. F. Allard and J. Szanyi, *Science*, 2009, **325**, 1670-1673.
33 A. Bruix, Y. Lykhach, A. Neitzel, N. Tsud, M. Vorokhta, V. Stetsovych, R. Fiala, K. C. Prince, V. Potin and F. Illas, *Angew. Chem. Int. Ed.*, 2014, **53**, 10525-10530.
34 W. Tang, Z. Hu, M. Wang, G. D. Stucky, H. Metiu and E. W. Mcfarland, *J. Catal.*, 2010, **273**, 125-137.
35 K. Asakura, S. Takakusagi, H. Ariga, W. J. Chun, S. Suzuki, Y. Koike, H. Uehara, K. Miyazaki and Y. Iwasawa, *Farad. Discuss.*, 2013, **162**, 710-711.
36 B. Qiao, J. Lin, A. Wang, Y. Chen, T. Zhang and J. Liu, *Chin. J. Catal.*, 2015, **36**, 1505-1511.
37 X. K. Gu, B. Qiao, C. Q. Huang, W. C. Ding, K. Sun, E. Zhan, T. Zhang, J. Liu and W. X. Li, *ACS Catal.*, 2014, **4**, 3886-3890.
38 Z. Huang, X. Gu, Q. Cao, P. Hu, J. Hao, J. Li and X. Tang, *Angew. Chem.*, 2012, **124**, 4274-4279.
39 G. Kyriakou, M. B. Boucher, A. D. Jewell, E. A. Lewis, T. J. Lawton, A. E. Baber, H. L. Tierney, M. Flytzani-Stephanopoulos and E. C. Sykes, *Science*, 2012, **335**, 1209-1212.
40 G. Pei, X. Liu, A. Wang, A. F. Lee, M. A. Isaacs, L. Li, X. Pan, X. Yang, X. Wang and Z. Tai, *ACS Catal.*, 2015, **5**, 3717-3725.
41 Y. Li, Z. Zhou, G. Yu, W. Chen and Z. Chen, *J. Phys. Chem. C*, 2010, **114**, 6250-6254.
42 E. H. Song, Z. Wen and Q. Jiang, *J. Phys. Chem. C*, 2011, **115**, 3678-3683.
43 Y. Tang, Z. Yang and X. Dai, *Phys. Chem. Chem. Phys.*, 2012, **14**, 16566-16572.
44 S. Sun, G. Zhang, N. Gauquelin, N. Chen, J. Zhou, S. Yang, W. Chen, X. Meng, D. Geng and M. N. Banis, *Sci. Rep.*, 2013, **3**, 1775-1783.
45 T. Eelbo, M. Waśniowska, P. Thakur, M. Gyamfi, B. Sachs, T. O. Wehling, S. Forti, U. Starke, C. Tieg and A. I. Lichtenstein, *Phys. Rev. Lett.*, 2013, **110**, 136804-136807.
46 Y. Tang, X. Dai, Z. Yang, Z. Liu, L. Pan, D. Ma and Z. Lu, *Carbon*, 2014, **71**, 139-149.
47 F. Li, J. Zhao and Z. Chen, *J. Phys. Chem. C*, 2012, **116**, 2507-2514.
48 P. Wu, P. Du, H. Zhang and C. Cai, *Phys. Chem. Chem. Phys.*, 2015, **17**, 1441-1449.

49 G. Vilé, D. Albani, M. Nachtegaal, Z. Chen, D. Dontsova, M. Antonietti, N. López and J. Pérez-Ramírez, *Angew. Chem. Int. Ed.*, 2015, **54**, 11265-11269.
50 X. Zhang, J. Lei, D. Wu, X. Zhao, Y. Jing and Z. Zhou, *J. Mater. Chem. A*, 2016, **4**, 4871-4876.
51 Y. Li and Q. Sun, *Sci. Rep.*, 2014, **4**, 795-798.
52 D. W. Ma, Q. Wang, X. Yan, X. Zhang, C. He, D. Zhou, Y. Tang, Z. Lu and Z. Yang, *Carbon*, 2016, **105**, 463-473.
53 S. Sinthika, E. M. Kumar and R. Thapa, *J. Mater. Chem. A*, 2014, **32**, 12812-12820.
54 P. Zhao, Y. Su, Y. Zhang, S. J. Li and G. Chen, *Chem. Phys. Lett.*, 2011, **515**, 159-162.
55 S. Lin, X. Ye, R. S. Johnson and H. Guo, *J. Phys. Chem. C*, 2013, **117**, 17319-17326.
56 K. Mao, L. Li, W. Zhang, Y. Pei, X. C. Zeng, X. Wu and J. Yang, *Sci. Rep.*, 2014, **4**, 5441-5448.
57 S. Lin, X. Ye and J. Huang, *Phys. Chem. Chem. Phys.*, 2014, **17**, 888-895.
58 C. Huang, X. Ye, C. Chen, S. Lin and D. Xie, *Comput. Theor. Chem.*, 2013, **1011**, 5-10.
59 X. Zhang, J. Guo, P. Guan, C. Liu, H. Huang, F. Xue, X. Dong, S. J. Pennycook and M. F. Chisholm, *Nat. Commun.*, 2013, **4**, 54-56.
60 S. Guo, X. Pan, H. Gao, Z. Yang, J. Zhao and X. Bao, *Chem-Eur. J.*, 2010, **16**, 5379-5384.
61 J. Deng, P. Ren, D. Deng, L. Yu, F. Yang and X. Bao, *Energ. Environ. Sci.*, 2014, **7**, 1919-1923.
62 P. M. Ajayan, T. W. Ebbesen, T. Ichihashi, S. Iijima, K. Tanigaki Amp and H. Hiura, *Nature*, 1993, **362**, 522-525.
63 C. Guerret-Piécourt, Y. L. Bouar, A. Lolseau and H. Pascard, *Nature*, 1994, **372**, 761-765.
64 J. P. Tessonnier, O. Ersen, G. Weinberg, C. Phamhuu, D. S. Su and R. Schlögl, *ACS Nano*, 2009, **3**, 2081-2089.
65 D. Ugarte, A. Chatelain and W. A. de Heer, *Science*, 1996, **274**, 1897-1899.
66 X. Pan, Z. Fan, W. Chen, Y. Ding, H. Luo and X. Bao, *Nat. Mater.*, 2007, **6**, 507-511.
67 W. Chen, Z. Fan, X. Pan and X. Bao, *J. Am. Chem. Soc.*, 2008, **130**, 9414-9419.
68 N. G. Chopra and A. Zettl, *Solid State Commun.*, 1998, **105**, 297-300.
69 C. W. Chang, W. Q. Han and A. Zettl, *Appl. Phys. Lett.*, 2005, **86**, 173102-173104.
70 C. Jin, F. Lin, K. Suenaga and S. Iijima, *Phys. Rev. Lett.*, 2009, **102**, 195505-195508.
71 A. Zobelli, C. P. Ewels, A. Gloter, G. Seifert, O. Stephan, A. S. Csillag and C. Colliex, *Nano Lett.*, 2006, **6**, 1955-1960.
72 G. Kresse and J. Hafner, *Phys. Rev. B: Condens. Matter*, 1993, **47**, 558-561.
73 G. Kresse and D. Joubert, *Phys. Rev. B: Condens. Matter*, 1999, **59**, 1758-1775.
74 G. Kresse and J. Furthmüller, *Comp. Mater. Sci.*, 1996, **6**, 15-50.
75 H. J. Monkhorst, *Phys. Rev. B*, 1976, **13**, 5188-5192.
76 G. Henkelman, *J. Chem. Phys.*, 2000, **113**, 9901-9904.
77 S. Grimme, *J. Chem. Phys.*, 2010, **132**, 154104-154119.
78 C. Campañá, B. Mussard and T. K. Woo, *J. Chem. Theory Comput.*, 2009, **5**, 2866-2878.
79 Y. Zhang, Q. Shi, Y. Liu, Y. Wang, Z. Meng, C. Xiao, K. Deng, D. Rao and R. Lu, *J. Phys. Chem. C*, 2015, **119**, 19826-19831.
80 Z. Meng, X. Zhang, Y. Zhang, H. Gao, Y. Wang, Q. Shi, D. Rao, Y. Liu, K. Deng and R. Lu, *ACS Appl. Mater. Inter.*, 2016, **8,** 28166-28170.
81 Z. Tian, S. Dai and D. Jiang, *ACS Appl. Mater. Inter.*, 2015, **7,** 13073-13079.
82 C. Y. Won and N. R. Aluru, *J Am Chem. Soc.*, 2007, **129**, 2748-2749.
83 Z. Zhang, H. Zhang, Y. Zheng, L. Wang and J. Wang, *Phys. Rev. B*, 2008, **78,** 035439-035444.
84 S. Abdel Aal, *Surf. Sci.*, 2015, **644**, 1-12.
85 Y. H. Lu, M. Zhou, C. Zhang and Y. P. Feng, *J. Phys. Chem. C*, 2009, **113**, 20156-20160.
86 K. H. Warnick, B. Wang, D. E. Cliffel, D. W. Wright, R. F. Haglund and S. T. Pantelides, *Nano Lett.,* 2013, **13**, 798-802.

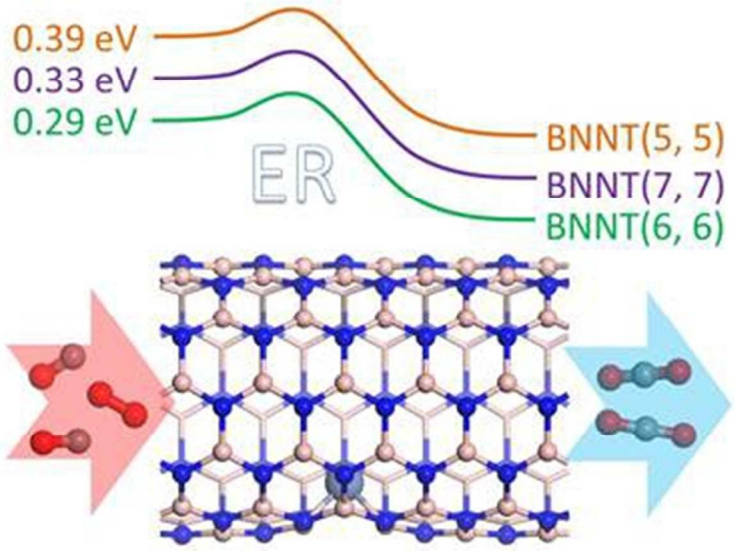

65x49mm (150 x 150 DPI)